OPEN BIOLOGY

royalsocietypublishing.org/journal/rsob

Research

Cite this article: Downton P, Dickson SH, Ray DW, Bechtold DA, Gibbs JE. 2024 Fibroblast-like synoviocytes orchestrate daily rhythmic inflammation in arthritis. *Open Biol.* **14**: 240089. https://doi.org/10.1098/rsob.240089

Received: 9 April 2024
Accepted: 7 June 2024

Subject Areas:
immunology, cellular biology

Keywords:
rheumatoid arthritis, circadian clock, inflammation, matrix metalloprotease, fibroblast-like synoviocytes

Authors for correspondence:
Polly Downton
e-mail: polly.downton@manchester.ac.uk
David A. Bechtold
e-mail: david.bechtold@manchester.ac.uk
Julie E. Gibbs
e-mail: julie.gibbs@manchester.ac.uk

Electronic supplementary material is available online at https://doi.org/10.6084/m9.figshare.c.7303177.

THE ROYAL SOCIETY PUBLISHING

Fibroblast-like synoviocytes orchestrate daily rhythmic inflammation in arthritis

Polly Downton[1], Suzanna H. Dickson[1], David W. Ray[2,3], David A. Bechtold[1] and Julie E. Gibbs[1]

[1]Centre for Biological Timing, Faculty of Biology, Medicine and Health, University of Manchester, Manchester M13 9PT, UK
[2]NIHR Oxford Health Biomedical Research Centre and NIHR Oxford Biomedical Research Centre, John Radcliffe Hospital, Oxford OX3 9DU, UK
[3]Oxford Centre for Diabetes, Endocrinology and Metabolism, and Oxford Kavli Centre for Nanoscience Discovery, University of Oxford, Oxford OX3 7LE, UK

PD, 0000-0002-1617-6153; DWR, 0000-0002-4739-6773; DAB, 0000-0001-8676-8704; JEG, 0000-0002-4248-2947

Rheumatoid arthritis is a chronic inflammatory disease that shows characteristic diurnal variation in symptom severity, where joint resident fibroblast-like synoviocytes (FLS) act as important mediators of arthritis pathology. We investigate the role of FLS circadian clock function in directing rhythmic joint inflammation in a murine model of inflammatory arthritis. We demonstrate FLS time-of-day-dependent gene expression is attenuated in arthritic joints, except for a subset of disease-modifying genes. The deletion of essential clock gene *Bmal1* in FLS reduced susceptibility to collagen-induced arthritis but did not impact symptomatic severity in affected mice. Notably, FLS *Bmal1* deletion resulted in loss of diurnal expression of disease-modulating genes across the joint, and elevated production of MMP3, a prognostic marker of joint damage in inflammatory arthritis. This work identifies the FLS circadian clock as an influential driver of daily oscillations in joint inflammation, and a potential regulator of destructive pathology in chronic inflammatory arthritis.

1. Introduction

Rheumatoid arthritis (RA) is a chronic, debilitating disease which affects 0.5–1% of adults in Western populations and requires long-term management [1]. Autoimmune activation leads to immune cell infiltration to the joint and inflammation of the synovial membrane. This results in local and systemic production of inflammatory cytokines and disease effector proteins including matrix metalloproteases, and subsequent progressive destruction of articular cartilage and bone. The associated pain, swelling and loss of mobility have profound impacts on quality of life. Individuals with RA typically show time-of-day differences in the severity of these symptoms, associated with diurnal rhythms in inflammatory mediators and circulating cytokines [2]. The mechanisms and cell types which drive this strong daily rhythmicity in disease activity remain to be fully defined. The circadian biological clock has been strongly implicated [3–5], and disruption of internal timing by lifestyle factors such as shift work is associated with elevated disease incidence [6].

The circadian system orchestrates daily rhythmic fluctuations across much of mammalian behaviour and physiology. At a molecular level, entraining signals (such as light, activity and nutrition) regulate the rhythmic expression of core clock transcription factors (TFs). These TFs interact through coordinated transcription–translation feedback loops that cycle with a period of close to 24 h [7]. The core circadian TFs additionally regulate numerous downstream target genes, giving rise to daily rhythms in cellular and physiological

processes including metabolism, immune homeostasis and inflammatory response. This internal daily rhythm impacts disease processes involved in chronic inflammatory conditions, such as asthma and arthritis [8,9].

Murine collagen-induced arthritis (CIA) is a well-established model of autoimmune, destructive, chronic arthritis, provoked by immunization against type II collagen [10]. Our previous work has demonstrated the circadian rhythmicity of human disease is recapitulated in the CIA model, with clear time-of-day-dependent fluctuation in the severity of joint inflammation [4,11]. Here, inflammatory gene expression in the joint and the abundance of associated circulating cytokines both peak during the rest phase for nocturnal mice, in agreement with human symptomatic peaks in the early morning. Our studies have also revealed that CIA-affected animals exhibit robust rhythmic gene expression in inflamed joint tissue, but this rhythmic transcriptional profile is profoundly different from that observed in naive joints [11]. Interestingly, analyses of immune cell infiltration into the diseased joints reveal only limited time-dependent differences in cell number and subtype, as well as pronounced suppression of core clock function in infiltrating myeloid cells [12]. This suggests that rhythmicity within the inflamed joint is driven by other joint-resident cell populations.

Fibroblast-like synoviocytes (FLS) are mesenchymal-derived cells that reside in the joint synovial space and have important roles in the maintenance, repair and immune homeostasis of healthy joints [13,14]. During inflammatory arthritis, FLS undergo extensive functional remodelling and drive tissue damage and inflammatory pathology. A number of FLS subpopulations have been identified in humans and mice [15–17], with distinct cell surface marker expression profiles and phenotypic properties. In chronic joint disease, lining layer (LL) FLS are typically associated with the expression of genes which contribute to destructive processes in the joint, while the sublining layer (SLL) cells are associated with the production of inflammatory signals and immune cell recruitment [15]. We have previously shown that FLS exhibit a robust internal circadian clock, and that modifying clock function can alter their inflammatory response [3,4]. These properties prompted us to hypothesize that joint-resident FLS may be a cellular driver of daily rhythms in inflammatory arthritis.

Here, we investigated FLS rhythmicity under normal conditions and in the context of CIA. Transcriptional profiling of FLS from naive and CIA-affected joints revealed a pronounced attenuation of time-of-day-dependent gene expression in response to disease. Nevertheless, a small, but potentially influential, subset of disease-related genes became robustly rhythmic in these cells. Upon deletion of the essential clock gene *Bmal1* in *Col6a1*-expressing FLS, we found a reduced incidence of CIA. However, in animals that progressed to severe disease, FLS-selective deletion of *Bmal1* led to a loss of time-of-day variation in markers of disease activity across the whole joint, supporting an important role for the FLS clock in the modulation of inflammatory processes and daily rhythms in joint disease.

2. Results

2.1. FLS exhibit altered rhythmic activity during CIA

To examine rhythmic transcriptional processes in FLS, we isolated Podoplanin (PDPN)-positive cells from naive and inflamed paws of wildtype DBA/1 mice at the peak and trough of disease activity (mid-light/rest phase, zeitgeber time ZT4, and mid-dark/active phase, ZT16; figure 1*a,b*). We found clear changes in gene expression in response to disease, with more than 8000 genes showing significant differential expression (DE) at each time point (figure 1*c*; electronic supplementary material, table S1 and dataset S1). Pathway analysis identified an enrichment of DE genes associated with KEGG pathways including '*rheumatoid arthritis*' and '*cytokine–cytokine receptor interaction*' (electronic supplementary material, figure S1*a*, table S2 and dataset S1), as would be expected. Time-of-day comparisons identified 1276 DE genes in FLS isolated from naive mice, highlighting that these joint resident cells exhibit significant diurnal variation in function under homeostatic conditions (electronic supplementary material, table S1 and dataset S1). Gene enrichment analyses included pathways associated with '*steroid biosynthesis*' and '*circadian rhythm*' (electronic supplementary material, table S2 and dataset S1). In contrast, we identified only 17 genes with significant DE between ZT4 and ZT16 in FLS isolated from inflamed joints (electronic supplementary material, table S1). This profound loss of time-of-day-dependent gene expression in response to CIA was not owing to increased intragroup variability in samples isolated from CIA mice, or to a relatively minor reduction in the magnitude of expression change between time points in naive and CIA-derived FLS (figure 1*d*; electronic supplementary material, figure S1*b*). This suggests a genuine and pronounced loss of rhythmic gene expression within FLS in the inflamed joint.

The group of genes which showed a significant time-of-day difference in FLS isolated from arthritic joints included a number encoding disease effector proteins including *Nos2* and *Mmp3* (figure 1*e*). These showed increased expression in CIA, with a notable emergence of time-of-day variation in expression, peaking at maximal disease activity (ZT4). These disease effectors have both previously been identified as being produced by synovial cells and chondrocytes in arthritis, with contributions to joint remodelling [18–21]. While failing to reach our stringent false discovery rate (FDR) criterion, a number of other inflammation-associated chemokines and disease effector genes, including *Tnfsf11* (RANKL), *Mmp13*, *Ccl20* and *Cxcl5*, were significantly upregulated in CIA FLS on *post hoc* analysis, with higher expression at the peak of disease activity (electronic supplementary material, figure S1*c*). Genes that remained robustly rhythmic in FLS from arthritic joints included circadian clock factors *Nr1d1* and *Cry1* (figure 1*f*). Interestingly, the impact of CIA was not uniform across the components of the molecular clock; genes associated with the negative regulatory arm of the clock (e.g. *Nr1d1*, *Cry1* and *Per2*) continued to show clear temporal expression, albeit at a reduced level, but positive regulators (e.g. *Bmal1*, *Npas2* and *Rora*) did not show time-of-day-dependent expression in CIA (figure 1*f*).

We have previously reported that CIA results in a profound alteration to gene expression in whole joints, including the emergence of a broad rhythmic transcriptional profile [11]. As this contrasts with our observed FLS gene expression patterns,

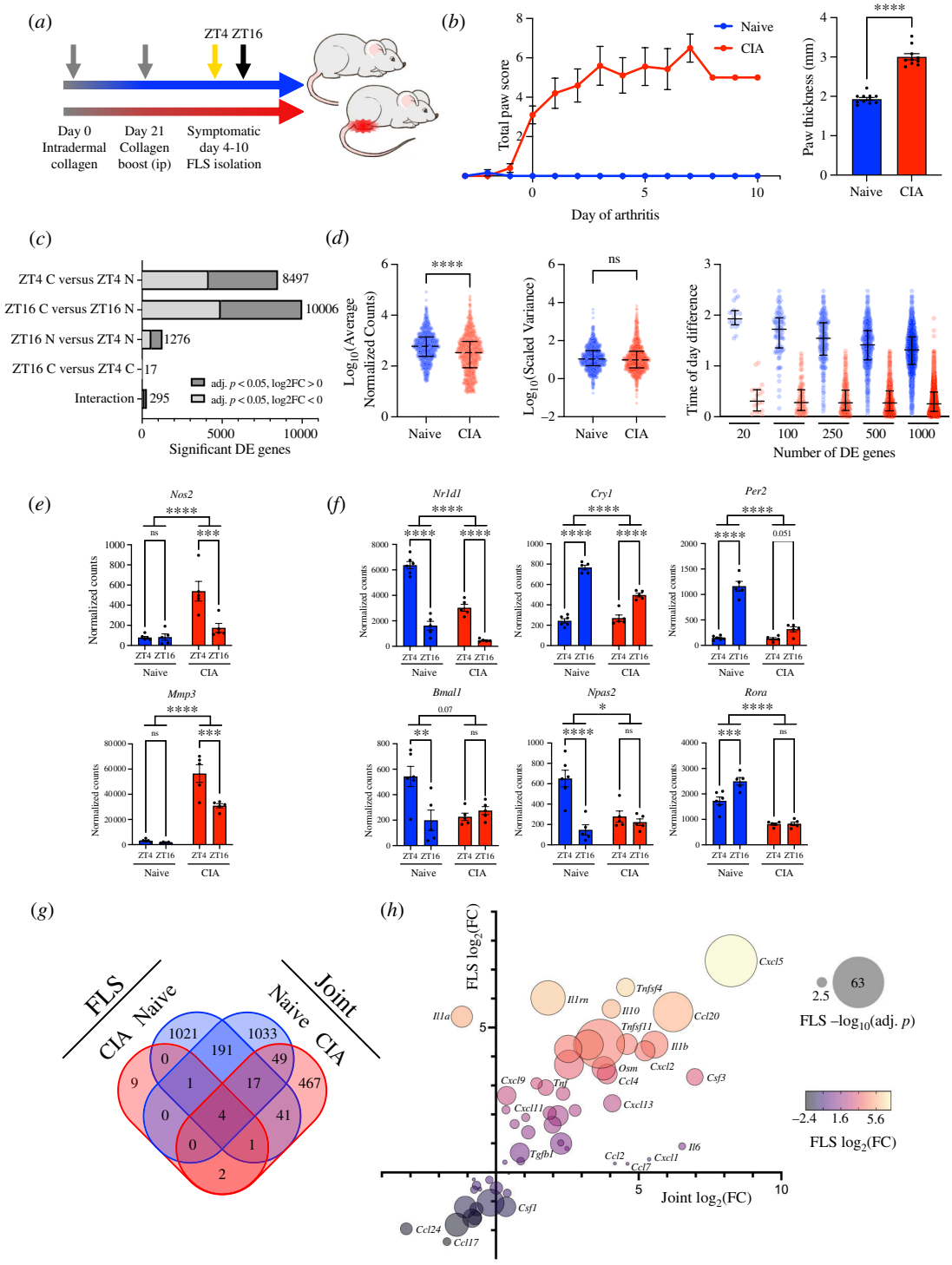

Figure 1. FLS exhibit altered rhythmic activity during CIA. (*a*) Schematic representation of CIA experimental plan. (*b*) Total paw score and paw thickness (day of sample collection) measurements of mice used for FLS isolation. Mean ± s.e.m., Welch's *t*-test, $n = 10–11$ per condition. (*c*) FLS from CIA or naive mice were isolated at ZT4 or ZT16 and analysed by RNAseq ($n = 5–6$ per time per condition). DE analysis identified transcripts which are significantly up- or downregulated with disease and/or time. (*d*) Peak expression level (left) and scaled variance (centre) were compared for the top 1000 significantly differentially expressed genes in naive or CIA FLS, and the magnitude of time-of-day difference calculated (right; difference in mean expression level at ZT4 and ZT16 after z-scoring for top 1000 genes rhythmic in naive FLS). Error bars show median ± interquartile range, distributions compared by Welch's *t*-test. (*e*) *Nos2* and *Mmp3* show time-of-day-dependent expression in FLS from inflamed joints. Mean ± s.e.m., two-way ANOVA treatment effect and time-dependent differences are indicated. $n = 5–6$. (*f*) FLS core clock gene expression in cells isolated from inflamed paws. Mean ± s.e.m., two-way ANOVA. (*g*) Four-way Venn comparison of time-of-day-dependent gene expression between ZT4 and ZT16 timepoints in FLS RNAseq and whole joint RNAseq datasets [11]. (*h*) Comparison of cytokine/chemokine expression changes with CIA in joints and isolated FLS. Of 92 transcripts considered (CCL, CXCL, interleukin, interferon, TNF and TGF families), 81 were detected and 58 were differentially expressed with CIA in at least one sample type. Fold changes (FC) in expression were calculated from RNAseq data at ZT4; bubble size represents the significance of DE between CIA and naive FLS.

we compared FLS-specific and whole joint transcriptional profiles in response to disease and time-of-day. We found that fewer than 10% of genes exhibiting time-dependent expression (significant DE in at least one condition) were common to FLS and whole joint datasets (figure 1*g*; electronic supplementary material, figure S1*d*). Indeed, almost 600 genes showed time-of-day differences with CIA in bulk joint samples (figure 1*g*), including mediators of inflammatory signalling (*Stat3*) and cytokines

(*Cxcl1*, *Il6* and *Ccl2*). We interpret this as representing time-of-day variation in expression of genes by non-FLS populations in the inflamed joint (e.g. immune cells). In support, the comparison of FLS versus bulk joint expression of these rhythmic cytokines demonstrated limited disease-induced expression within FLS but a substantial increase in expression within the joint as a whole (figure 1*h*; electronic supplementary material, table S3). For example, *Il6* and *Cxcl1* are highly rhythmic and strongly induced in the whole joints (electronic supplementary material, figure S1*e*), but this is not replicated in purified FLS, where CIA-induced expression is relatively limited. Of note, IL6 levels are also highly rhythmic in the circulation of both arthritic mice and humans [11,22]. This suggests that FLS are not the primary source of these signals.

2.2. Loss of molecular clock function alters FLS transcriptional profile

Although FLS lost substantial transcriptional rhythmicity in arthritic joints, some important factors exhibited robust rhythmicity in these cells, including mediators which may be involved in communicating circadian timing and inflammatory state to other cell populations within the joint. We next assessed the role of FLS circadian oscillator function in disease pathogenesis using transgenic mice with selective deletion of the essential core circadian gene *Bmal1* in mesenchymal cells, including FLS, using the established *Col6a1*-cre driver line [3,23]. The resulting mice (*Col6a1*$^{Cre+}$*Bmal1*$^{fl/fl}$) were backcrossed onto a DBA/1 background to promote susceptibility to the CIA model of inflammatory arthritis. Targeting was confirmed in FLS isolated from *Cre*-expressing mice (*Cre*+), which showed a significant reduction in *Bmal1* transcript and protein expression compared with *Bmal1*$^{fl/fl}$ littermate controls (*Cre*-; figure 2*a,b*).

To ensure that *Col6a1*-cre targeting was effective across FLS subpopulations, we analysed gene expression in CD45$^-$CD31$^-$PDPN$^+$ cells sorted based upon CD90.2 expression, a marker that allows distinction between SLL (CD90.2$^+$) and LL (CD90.2$^-$) FLS. We found comparable expression of *Cre* recombinase in sorted LL and SLL cell populations from *Cre*+ mice (figure 2*c*). In addition, we crossed *Cre*+ mice with a line of mice that provide *Cre*-dependent EYFP expression and found similarly robust EYFP fluorescence in LL and SLL cells (electronic supplementary material, figure S2*a*). These data demonstrate effective targeting by the *Col6a1*-cre driver across FLS subpopulations.

We next used single-cell RNA sequencing (scRNAseq) to characterize joint-derived PDPN$^+$ cell identity and determine the impact of *Bmal1* deletion on FLS transcriptional phenotype. We identified multiple FLS subpopulations, and only minor contamination by other cell types (figure 2*d*; electronic supplementary material, figure S2*b–d*). Overall, cellular subpopulation distributions in *Cre*+ and *Cre*− FLS were broadly similar (figure 2*d*) and in line with previous work [14,16,17], indicating that *Bmal1* expression is not required for differentiation of FLS subsets. We used a pseudo-bulk DE analysis approach to assess the impact of *Bmal1* deletion across all FLS populations. This identified 603 DE genes between *Cre*+ and *Cre*− FLS (figure 2*e*; electronic supplementary material, table S4 and dataset S2). Ontology analysis identified a number of enriched KEGG pathways, including '*extracellular matrix (ECM)–receptor interactions*' and '*circadian rhythms*' (figure 2*f*; electronic supplementary material, table S5 and dataset S2). In line with this, FLS lacking *Bmal1* exhibited the expected altered expression of core clock genes (figure 2*g*). We also observed altered expression of numerous ECM factors including collagens (figure 2*g*) highlighting a potential role for the FLS clock in regulating ECM dynamics in the healthy joint.

2.3. Mice lacking *Bmal1* expression in FLS show altered CIA development and loss of rhythmic joint inflammation

To understand the impact of clock ablation on disease phenotype, we next characterized the development and severity of CIA in *Cre*+ mice and *Cre*− littermate controls. Interestingly, we found a significant reduction in the incidence of disease in *Cre*+ mice (figure 3*a*; electronic supplementary material, figure S3*a,b*). This was despite comparable anticollagen IgG1 and IgG2a antibody responses, confirming the ability of both genotypes to mount a competent immune response to collagen immunization (figure 3*b*). The cause of the reduced susceptibility to symptomatic disease is unclear but may result from cellular or structural changes within the joint. Our earlier work in C57BL/6J mice showed that similar deletion of *Bmal1* in *Col6a1*-expressing cells leads to age-related joint stiffening and increased chondrocyte number and paw thickness [3]. Here, we also observe a small but significant increase in paw thickness in naive *Cre*+ mice compared with age-matched *Cre*− littermate controls (electronic supplementary material, figure S3*c*). Elevated collagen gene expression by FLS which lack *Bmal1* expression (figure 2*g*) may contribute to both altered joint matrix and antigen response.

Importantly, no significant differences were observed in markers of disease severity (paw score, paw thickness) between *Cre*+ and *Cre*− animals which went on to develop arthritis (figure 3*c*). Therefore, to determine the impact of FLS *Bmal1* deletion on established joint disease, our subsequent analyses compare joints from symptomatic CIA mice with severe disease (paw score of ≥ 3). In comparison to joints isolated from naive and asymptomatic mice, CIA caused a significant increase in infiltrating immune cells (predominantly neutrophils); this was similar between *Cre*+ and *Cre*− genotypes and did not show a time-of-day difference (figure 3*d,e*). Moreover, no genotype differences were observed in PDPN$^+$ cell number (as a fraction of non-immune cells), the proportion of LL and SLL cells, or the expression of disease-associated FLS activation markers including CD106 (VCAM1) and FAPα in naive or CIA paws (figure 3*f*; electronic supplementary material, figure S3*d*). Taken together, these data suggest that once disease is established, *Cre*+ mice exhibit a similar profile of immune cell and FLS activation within affected joints to their control littermates.

To determine whether the intrinsic clock function of FLS contributes to setting wider daily rhythms in inflammation across the whole joint, we isolated RNA from inflamed (CIA) and naive whole joints of *Cre*+ mice and *Cre*− littermate controls. We observed the expected significant elevation in proinflammatory gene expression in CIA joints; however, time-of-day variation in expression of key inflammatory cytokines (*Cxcl1*, *Il6*, *Il1b*) was found in *Cre*− but not *Cre*+ joints (figure 4*a*). This suggests that

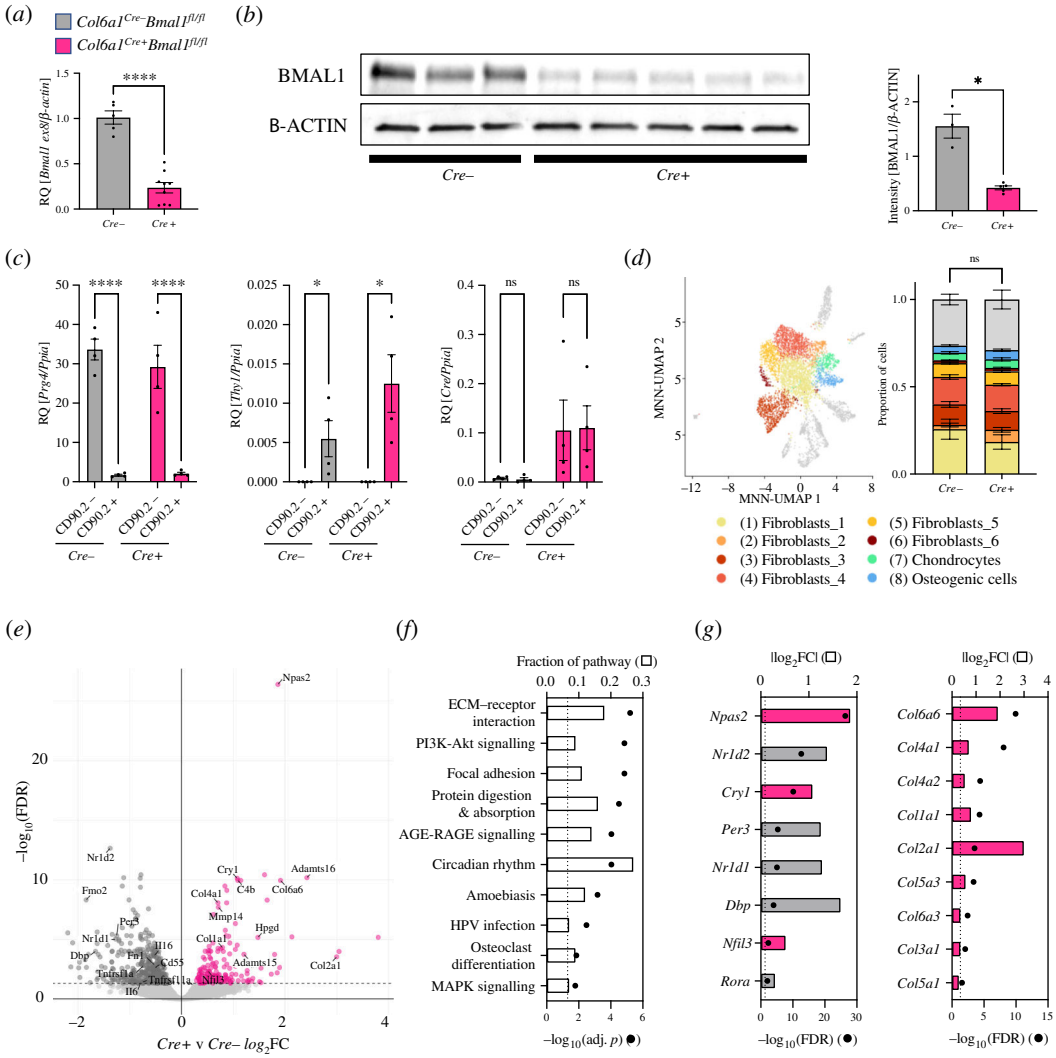

Figure 2. Loss of molecular clock function alters FLS transcriptional profile. (*a,b*) Quantification of BMAL1 ablation at transcript (*a*) and protein (*b*) levels for *Cre*− and *Cre*+ mice. Mean ± s.e.m., Welch's *t*-test, $n = 3$–7 per genotype. (*c*) FLS sorted into CD90.2− and CD90.2+ subpopulations were analysed to confirm LL versus SLL identity (*Prg4* and *Thy1* marker gene expression, respectively; left, centre) and comparable expression of Cre recombinase (right). Gene expression is presented as mean ± s.e.m., RM two-way ANOVA, *post hoc* subpopulation comparison, $n = 4$ independent replicates. (*d*) Gene expression of FLS isolated from joints was analysed using split pool ligation-based transcriptome sequencing (SPLIT-seq). Cells were clustered (left) and subpopulation identity determined based on cluster-specific expression of highly variable genes, identifying six FLS subpopulations (as well as chondrocytes, osteogenic cells and minor populations of other cell types), with no significant difference in population distribution between genotypes (right); two-way ANOVA, $n = 3$ per genotype. (*e*) Volcano plot showing differential gene expression between naive *Cre*− (grey) and *Cre*+ (pink) samples. Comparative expression analysis using edgeR considered pseudo-bulk populations of cells from clusters 1–8. (*f*) Analysis of genes showing significant DE between genotypes identified enriched KEGG pathways (adj. $p < 0.05$, dashed line). Fraction of pathway indicates the proportion of genes associated with a pathway which showed significant DE between genotypes. (*g*) Circadian (left) and collagen/cell matrix-associated genes (right) are differentially expressed between genotypes (FDR < 0.05, dashed line). DE is presented as the absolute value of $\log_2$ fold change, where grey indicates increased expression in *Cre*− mice and pink indicates increased expression in *Cre*+ mice. HVG, highly variable gene.

the FLS clock is necessary to confer rhythmicity. Since we find limited expression of these cytokine transcripts in FLS themselves (figure 1*h*; electronic supplementary material, figure S1e), this implicates FLS as orchestrators of disease rhythmicity across other resident or infiltrating cells.

CIA joints from *Cre*− mice exhibited a significant induction and time-of-day variation in *Mmp3* transcript (figure 4*a*). This time-of-day expression difference of *Mmp3* was lost in *Cre*+ joints, with elevated expression at the typical nadir of inflammation. Significant MMP activity can be observed in symptomatic CIA paws *in vivo* (figure 4*b*; electronic supplementary material, figure S4*a*). *Mmp3* expression was also persistently upregulated in FLS cultured from CIA paws (electronic supplementary material, figure S4*b*) and strongly induced in cultured FLS by proinflammatory cytokine treatment (electronic supplementary material, figure S4*c*). Analysis of plasma samples from CIA mice around the peak and nadir of arthritic inflammation revealed time-of-day differences in MMP3 levels at ZT6 compared with ZT18 in *Cre*− mice (figure 4*c*). In contrast, *Cre*+ mice exhibited the loss of time-of-day difference and augmented levels of MMP3 in plasma. Overall, this supports clock-dependent regulation of joint pathological processes by FLS.

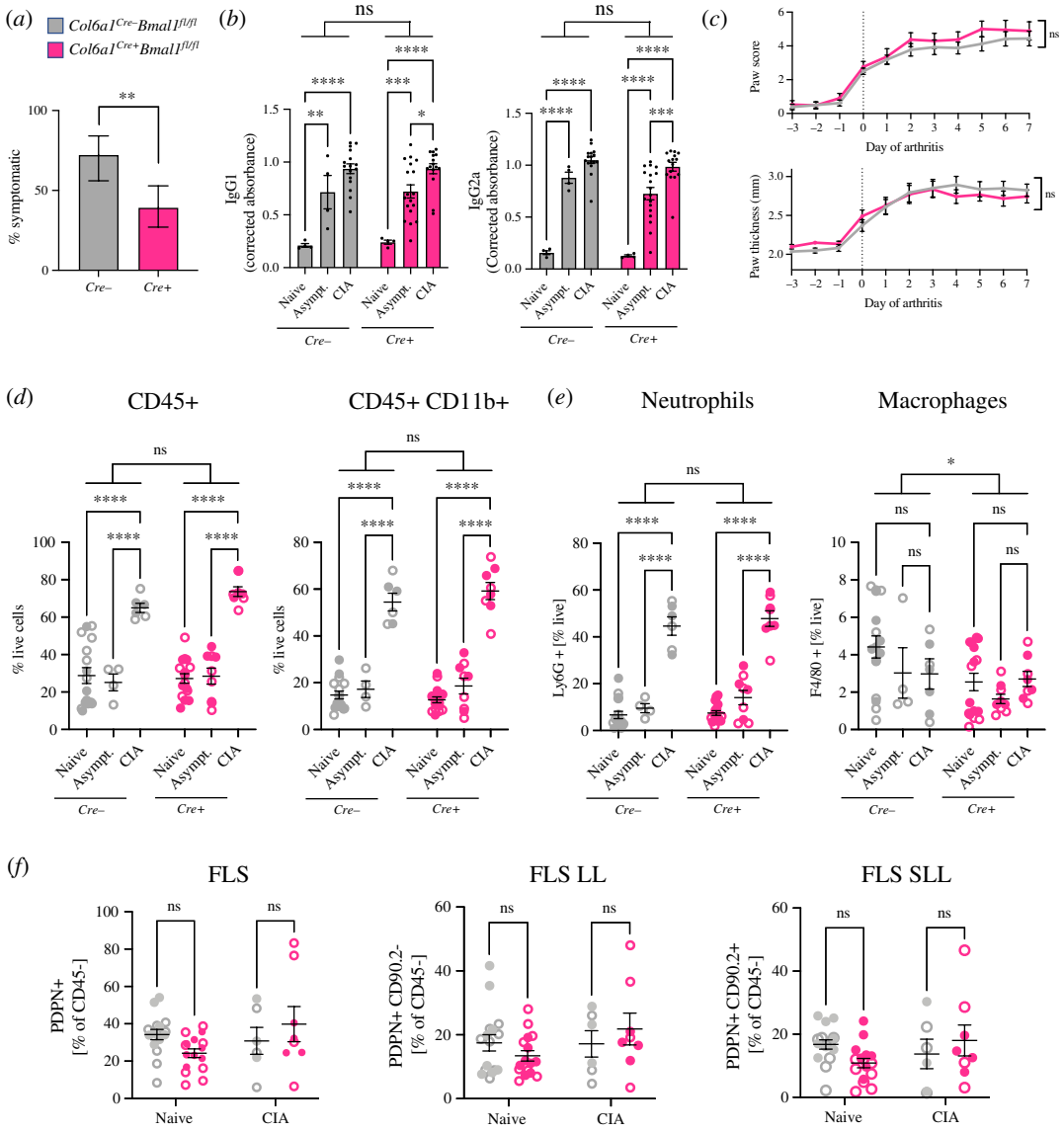

Figure 3. Mice lacking *Bmal1* expression in FLS show altered CIA development. (*a*) Development of symptoms in *Cre+* mice was significantly reduced compared with littermate *Cre–* controls. Fisher's exact test; error bars indicate 95% confidence interval. (*b*) Quantification of IgG1 and IgG2a anticollagen antibody response in plasma from naive, asymptomatic and symptomatic CIA mice. Two-way ANOVA, *post hoc* treatment comparison, $n = 4$–18 per condition. (*c*) Daily paw score (top) and thickness measurement (bottom) found no difference in disease severity between mice that develop symptoms. Two-way ANOVA, mean ± s.e.m., $n = 17$–26 mice/genotype. (*d,e,f*) Flow cytometry analysis of immune cell infiltration into joints with disease, comparing total immune cell proportion (*d*) and cell identity (*e*) between genotypes. Flow cytometry analysis of FLS identity (*f*) comparing LL versus SLL between disease and time-of-day. Open circles indicate ZT8 sample collection, filled circles indicate ZT20 sample collection. Two-way ANOVA, *post hoc* treatment (*d, e*) or genotype (*f*) comparison, $n = 3$–8 per time per condition.

3. Discussion

RA, like many chronic inflammatory conditions, shows a characteristic variation in severity by time-of-day. Understanding the interplay between autoimmune inflammation and internal biological timing offers an opportunity to improve the management of chronic disease and identify new therapeutic approaches. Our previous work demonstrated damping of core clock gene rhythmicity in major immune cell populations harvested from arthritic joints, despite robust oscillations in joint transcriptional activity and circulating cytokine levels [11,12]; hence, we hypothesized FLS, resident within the joint, might be a key source of these rhythmic inflammatory signals. FLS are a heterogeneous population of cells that are intimately involved in the pathogenesis of RA [24–27]. Here, we find that diurnal rhythmicity in FLS gene expression is also suppressed by chronic inflammation. However, a subset of disease-relevant genes gain significant rhythmicity in these cells. Genetic disruption of *Bmal1* within FLS prevents time-of-day-dependent variation of key arthritis effector molecules within inflamed joints. Together, these studies identify an important functional role for the clock within FLS in promoting rhythmic signatures associated with chronic inflammatory arthritis.

A suppressive effect of inflammation and inflammatory cytokine signals on circadian gene expression has been widely reported *in vivo* [11,28–30] and *in vitro* [31,32]. Transcriptional profiling of joint FLS from naive and CIA mice showed a widespread damping of time-of-day-dependent gene expression in these cells in response to arthritis. In contrast, prior whole joint sequencing revealed emergent inflammatory gene rhythmicity in diseased joints (in line with rhythmic symptoms). Importantly, *Col6a1*$^{Cre+}$*Bmal1*$^{fl/fl}$ murine CIA studies revealed that key rhythmic inflammatory signatures in whole joint were

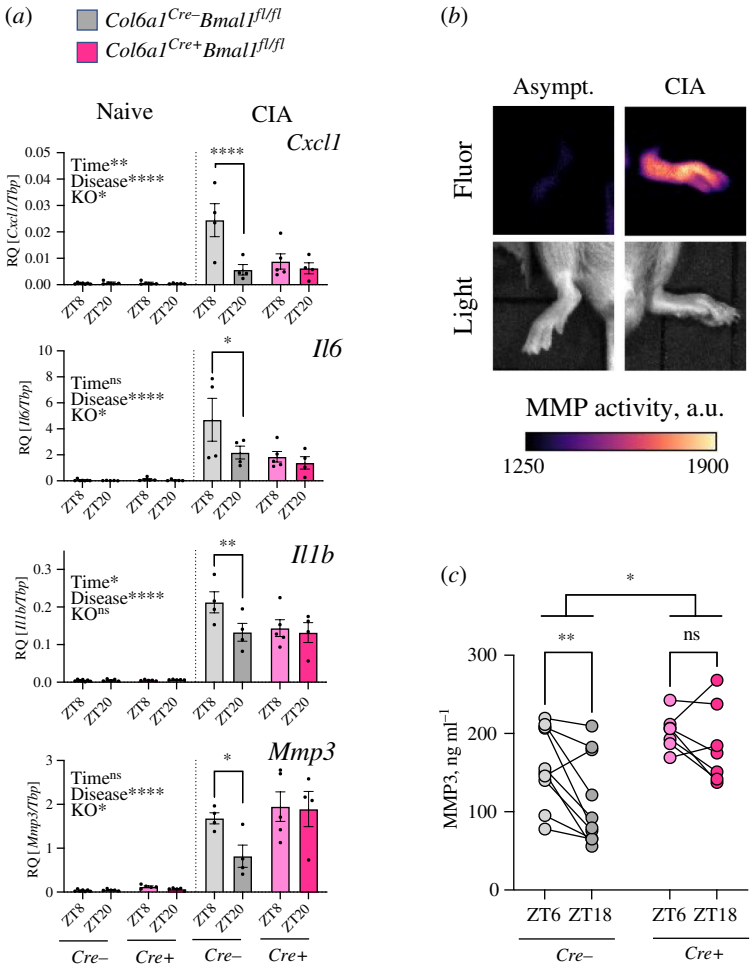

Figure 4. Mice lacking *Bmal1* expression in FLS lose rhythmicity of disease effectors in joints. (*a*) Inflammatory gene expression in naive and CIA joints from *Cre*– and *Cre*+ mice. Three-way ANOVA results and time-dependent differences in gene expression are indicated, $n = 4$–7 per condition. (*b*) Administration of an MMP activity-dependent fluorescent probe identified localised enzymatic activity in inflamed (but not asymptomatic) CIA paws. (*c*) MMP3 level in plasma from arthritic mice across time. RM two-way ANOVA with *post hoc* time comparison, $n = 7$–10 per genotype.

dependent on *Bmal1* expression in FLS. Thus, while FLS are not the cellular source of the inflammatory rhythmic signature in arthritic joints, clock function within these cells appears to be fundamental in driving these oscillations. Target cell types responsible for producing the rhythmic proinflammatory profile probably include cells of a myeloid lineage. Indeed, we have shown that despite significant damping of their own intrinsic cellular clock in an arthritic joint, myeloid cell proinflammatory outputs appear to be shaped by the daily changes in the surrounding joint environment [12]. In the current study, FLS sequencing has revealed candidate signals through which FLS may impose rhythmicity across the joint. These potentially include NO production via rhythms in *Nos2* expression and rhythmic MMP3 production, both previously linked to arthritis-associated joint damage and regulation of inflammation [18,33,34], as well as other inflammation-associated disease effectors (*Cxcl5*, *Ccl20*, *Mmp13*, *Rankl*/*Tnfsf11*). Further work is required to fully elucidate the mechanisms and cell types involved.

MMP proteins cause irreversible damage to cartilage and bone, resulting in ECM degradation in the inflamed joint [21,33,35–38]. MMP3 showed time-of-day differences in arthritic DBA/1 mice, with the highest expression at the peak of inflammatory symptoms. MMP3 shows similar time-of-day variation in human inflammatory disease contexts [39]. We find that the FLS clock restrains MMP3 production, leading to consistently high plasma concentrations in the absence of *Bmal1*. This is in line with previous studies showing altered MMP3 expression in global *Bmal1* KO mice [40] and *Bmal1*-dependent regulation of MMP production by chondrocytes [41]. In addition, modulation of the clock factor and BMAL1 target NR1D1 can repress production of MMP3 by FLS and reduce cartilage and bone loss in CIA [42], and there is evidence of direct regulation of MMP3 by NR1D1 in some cell types [43,44]. MMP3 is of particular clinical interest as a biomarker for inflammatory arthritis since serum level reflects synovial fluid level [45,46] and is a prognostic indicator of joint damage in human RA [47–49]. Targeting FLS-derived disease effectors has shown synergistic benefit in combination with standard RA treatments in preclinical trials [50–53], and therapeutic modulation of FLS function (rhythmic activity and MMP expression) may present an opportunity for diagnostic and therapeutic benefit.

Genetic disruption of core clock function has typically been associated with increased severity of inflammatory response [54–57]. Global deletion of *Nfil3*, *Cry1* and/or *Cry2* worsens disease severity in experimental arthritis models [58–60]. We have previously shown that in collagen antibody-induced arthritis (CAIA, a model which does not generate B- and T cell-mediated autoimmune responses [61]), *Bmal1* deletion in FLS resulted in increased neutrophil infiltration and elevated inflammatory gene expression in affected joints [3]. In the CIA model of autoimmune-mediated arthritis in the susceptible DBA/1 genetic background, *Bmal1* deletion in FLS led to a reduction in the incidence of disease compared with control littermates. This

may reflect differences in the genetic background of the mice, but more likely reflects differences in the immune mechanisms involved in disease induction between the two experimental arthritis models (CAIA and CIA). This would suggest that FLS, and *Bmal1* activity within these cells, are important in early immune priming events and/or initiation of the immune response at the joint synovium.

In a naive state, *Col6a1*$^{Cre+}$*Bmal1*$^{fl/fl}$ DBA/1 mice exhibit a small increase in paw thickness and enhanced FLS expression of collagens and other ECM-associated genes. This is in line with our previous work showing that ablation of *Bmal1* using the same *Col6a1*-cre driver in C57BL/6J mice results in joint stiffening [3]. *Bmal1* ablation in other tissue contexts has also been shown to alter ECM organization [62,63]. Together, these findings reveal a role for FLS BMAL1 activity or wider circadian clock function in shaping joint ECM dynamics, and we speculate that altered collagen expression and/or resulting joint architecture contribute to the attenuated susceptibility to CIA observed here. Indeed, several studies have found that prior dosing with soluble collagen can reduce CIA incidence, while administration after the development of symptoms can increase anti-inflammatory cellular response and reduce expression of proinflammatory markers [64–66].

In summary, we show that the FLS clock machinery is robust in healthy joints and directs a programme of rhythmic gene expression. However, that rhythmic activity is significantly attenuated during inflammation. Despite this attenuation, *Bmal1* expression in FLS is required for rhythmic expression of cytokines and other disease-effector molecules in the arthritic joint. As we find FLS are not the cellular source of many of the cytokines typically associated with rhythmic symptoms in RA, this demonstrates the role of FLS in driving rhythmic function in other immune populations of the diseased joint.

4. Material and methods

4.1. Animals

Mice were maintained in the University of Manchester Biological Services Facility. All procedures were approved by the University of Manchester Animal Welfare and Ethical Review Body and carried out according to the Animals (Scientific Procedures) Act 1986 under Home Office project licence numbers P000BBBC3 and PP5819195. Mice were group housed under a 12 h : 12 h light/dark cycle with *ad libitum* access to food and water. DBA/1 mice were purchased from Envigo (Huntingdon, UK). Transgenic mice created for this study were generated in-house. Male *Col6a1*$^{Cre+}$*Bmal1*$^{fl/fl}$PER2::LUC mice [3] were backcrossed with female DBA/1 mice for three generations, then interbred to obtain homozygosity of the *Bmal1*$^{fl/fl}$ modification. Ai32(RCL-ChR2(H134R)/EYFP) mice, which express a channel rhodopsin–EYFP fusion protein in *Cre*+ cells [67], were crossed with DBA/1 *Col6a1*$^{Cre+}$*Bmal1*$^{fl/fl}$PER2::LUC mice for *Cre*-expression mapping experiments. Primers used for genotyping are given in electronic supplementary material, table S6.

4.2. Primary cell isolation and culture

Paws were dissected to separate joints, then incubated with collagenase IV (10 mg ml^{-1}, Sigma C5138) in DMEM containing 10% FBS and 1% penicillin–streptomycin at 37°C with shaking for 2 h. Cells were maintained in DMEM containing 10% FBS and 1% penicillin–streptomycin in a humidified incubator (37°C, 5% CO_2). Cells between passages 3 and 7 were used for all experiments. For *in vitro* experiments, cells were treated with recombinant mouse IL1β (final concentration 10 ng ml^{-1}, Sigma–Aldrich I5271−5UG).

4.3. Collagen-induced arthritis (CIA)

CIA was induced in male mice (7–13 weeks) as described previously [11]. Initial intradermal administration of bovine type II collagen in Complete Freund's Adjuvant (MD Bioproducts, Zurich, 804001-sol and 501009) was followed by i.p. booster of collagen in saline on day 21. Disease severity and paw thickness were assessed daily. Disease severity was scored on a 4-point scale for each paw (1 for single inflamed digit, 2 for multiple inflamed digits, 3 for swelling of paw pad and 4 for severe swelling of paw pad and ankle/wrist joint) [4]. Terminal tissue samples were collected 7–10 days after the development of symptoms unless otherwise specified.

4.4. *In vivo* procedures

Small-volume blood samples were collected from the tail vein 5–7 days after the development of symptoms. Blood was collected into EDTA-coated tubes, and plasma was isolated by centrifugation at 3000 *g* for 10 min at 4°C. For *in vivo* imaging studies, MMP activity was assayed using MMPSense 750 FAST probe (Perkin–Elmer, NEV10168). Images were collected using an IVIS Lumina system (745 ex/800 em). After collection of a baseline image, the probe was administered IV (1.5–2 nmol), followed by image collection under isofluorane anaesthesia 12 h after probe administration.

Terminal blood was collected in MiniCollect K3EDTA tubes (Greiner Bio-One) and stored on ice prior to centrifugation at 3000 *g* for 10 min at 4°C. For whole joint RNA analysis, paws were dissected and skin removed prior to being flash frozen in liquid nitrogen. For FLS RNAseq and scRNAseq analysis, the skin was removed and the paw was incubated in cell culture media prior to joint digestion and FLS isolation.

4.5. FLS enrichment

Paws were dissected and incubated with collagenase IV (10 mg ml^{-1}, Sigma C5138) as described above. FLS for RNAseq and scRNAseq analysis were selected following 1–1.5 h collagenase digestion using the EasySep Release Mouse PE Positive Selection kit (Stemcell Technologies, 17656) and a PDPN–PE-conjugated antibody (BioLegend 127407). The efficiency of selection was tested by staining of released cells (or parallel unprocessed samples) for flow cytometry, and enrichment of the target cell population is shown in electronic supplementary material, figure S5*a*.

4.6. Flow cytometry and cell sorting

Joint cells for flow cytometry were isolated as described above, with 1–1.5 h collagenase digestion. Cells were passed through a 40 µm filter, washed with PBS, then subjected to subsequent incubations with live/dead stain (20 min at 4°C, eBioscience Fixable Viability Dye e780, Invitrogen 65-0865-14), Fc block (20 min at 4°C, eBioscience 14-0161-85), and extracellular antibody mix (1 h at 4°C; electronic supplementary material, table S7). Following extracellular antibody incubation, cells were washed once with FACS buffer (PBS containing 4% FBS and 10 mM EDTA), then fixed using an intracellular staining buffer set (eBioscience 00-5523). Cells were kept at 4°C until analysis, or subjected to intracellular antibody staining following overnight incubation in fixative. Where intracellular staining was necessary, cells were washed with permeabilization buffer, then incubated with primary intracellular antibody in permeabilization buffer (30 min at 4°C, electronic supplementary material, table S7). This process was repeated with a fluorescent secondary antibody if the primary antibody was unconjugated, and cells were resuspended in FACS buffer prior to analysis. *In vitro* cultured FLS were washed with PBS, detached using trypsin and resuspended in FACS buffer prior to staining using the same protocol. Stained cells were passed through a 40 µm filter and analysed on a BD LSRFortessa instrument. Compensation for spectral overlap used OneComp (eBioscience 01-1111-42) and ArC amine-reactive (Thermo Fisher A10346) compensation beads. Data were analysed using FlowJo v. 10. Gating strategies for flow and cell sorting experiments were set using fluorescence minus one control samples and are described in electronic supplementary material, figure S5*b–d*.

Joint cells for sorting were isolated as above, except the live/dead staining step was omitted. The antibody panel used for staining is described in electronic supplementary material, table S7. Cells were sorted into cold PBS using a BD FACSAria instrument. Immediately prior to sorting, 7-AAD (50 ng ml^{-1}, Biolegend 420404) was added to the filtered cell suspension. After sorting, cell pellets were collected by centrifugation and resuspended in buffer RLT Plus (Qiagen) prior to RNA isolation and analysis.

4.7. RNA isolation

RNA was extracted from PDPN-selected FLS and sorted FLS using the RNeasy Micro Plus kit (Qiagen). The FLS cell pellets were lysed in buffer RLT Plus supplemented with DTT, and RNA isolated according to the manufacturer's instructions. RNA integrity was assessed using a 4200 TapeStation (Agilent Technologies).

RNA was extracted from cultured FLS using the ReliaPrep Cell kit (Promega). Cells were cultured in 24 or 12 well plates. After the indicated treatment, cells were washed in cold PBS and then lysed by direct addition of buffer BL + TG to culture plate wells, followed by scraping and collection into microcentrifuge tubes. RNA was isolated according to the manufacturer's instructions.

RNA was extracted from whole joint samples using TRIzol. Tissue was ground with liquid nitrogen and then homogenized in a Lysing Matrix D tube using a BeadMill homogeniser (3 × 4 m/s for 40 s). RNA was extracted using chloroform and then precipitated with isopropanol. Isolated RNA was further purified using the RNeasy Micro Plus kit (Qiagen).

4.8. RNAseq

Sequencing library preparation and sequencing was performed by the University of Manchester Genomic Technologies Core Facility. Libraries were generated using the Stranded mRNA Prep Ligation kit (Illumina, Inc) according to the manufacturer's protocol. Libraries were pooled prior to loading onto an S1 flow cell for paired end sequencing (59 + 59 cycles, plus indices) on an Illumina NovaSeq6000 instrument. The binary base call (BCL) files were processed using the bcl2fastq software (v. 2.20.0.422).

4.9. scRNAseq

FLS were isolated using the EasySep Release PE positive selection kit and PDPN-PE antibody, as described above. Selected cells were fixed immediately after bead release using Cell Fixation reagents (Parse Biosciences SB1003) in accordance with the manufacturer's instructions. Fixed cell suspensions were counted using a haemocytometer before being flash-frozen in liquid nitrogen and stored at −80°C prior to barcoding and library preparation. Libraries for sequencing were prepared using the Evercode Whole Transcriptome Mini kit (Parse Biosciences EC-W01010). Briefly, fixed cells were barcoded by in-cell reverse transcription, with samples distributed between 12 wells containing specific barcoded primers, followed by two subsequent rounds of mixing and ligation (2 × 96 wells containing specific barcodes) to generate unique combinatorial barcodes for each cell. Cells were then lysed and barcoded cDNA isolated, amplified and cleaned for sequencing library generation. Library

fragment size and quality were assayed using a 4200 TapeStation (Agilent Technologies). Libraries were loaded onto an SP flow cell for paired-end sequencing (74:86, c/w 5% PhiX spike-in) on the Illumina NovaSeq6000 platform, and BCL files were processed as above.

4.10. Bioinformatic analysis of sequencing data

Bioinformatic analysis was undertaken in collaboration with the University of Manchester Bioinformatics Core Facility.

Sequencing quality was assessed using FastQC. FLS RNAseq data sequence adapters were removed and reads were quality trimmed using Trimmomatic_0.39 [68]. The reads were mapped against the reference mouse genome (mm10/GRCm38) and counts per gene were calculated using annotation from GENCODE M25 using STAR_2.7.7a [69]. Normalization, principal components analysis and DE were calculated with DESeq2_1.18.1 [70]. Adjusted *p*-values were corrected for multiple testing using the Benjamini and Hochberg method. Pathway analysis used the enrichR web portal to query the KEGG 2019 Mouse database [71]. For time-of-day/disease comparison of FLS and joint RNAseq datasets, previously published joint RNAseq data from samples collected at ZT4 and ZT16 were reanalysed using the same pipeline [11].

FLS single- cell FASTQ files were mapped against the Mouse reference GRCm39 and Ensembl annotation (v107) using the Parse Biosciences pipeline 'split-pipe' (v1.0.1p) to generate the gene-cell count matrix. These were processed in the R environment (v. 4.1) following the workflow of Amezquita *et al.* [72]. Briefly, the 'all-well' count matrix was imported into R to create a SingleCellExperiment object. A combination of median absolute deviation, as implemented by the 'isOutlier' function in scuttle (v. 1.4.0) [73] and exact thresholds were used to identify and subsequently remove low-quality cells. The expression values were log-normalized and the per-gene variance of the log-expression profile was modelled using the 'modelGeneVar' function and the top 1500 highly variable genes (HVGs) were identified using the 'getTopHVGs' function, both from scran (v. 1.22.1) [74]. Batch effects were corrected for visualisation using the mutual nearest neighbours (MNN) approach implemented by the 'fastMNN' function from batchelor (v. 1.10.0) [75]. The MNN corrected coordinates were used as input to produce the uniform manifold approximation and projection (UMAP) using the 'runUMAP' function from scater (v. 1.22.0), respectively. Cell subpopulations were clustered using the Leiden algorithm from igraph (v. 1.3.0). Marker genes were identified using the 'findMarkers' function from the scran R package. DE analysis between WT and KO populations was performed on pseudo-bulk samples from clusters 1 to 8 using the quasi-likelihood pipeline from edgeR (v. 3.36.0) [76,77]. Genes with a FDR below 5% were considered differentially expressed.

4.11. Quantitative PCR

RNA was converted to cDNA using the GoScript Reverse Transcriptase System (Promega A5001). Quantitative PCR used KAPA SYBR fast universal mix (Kapa Biosystems KK4602) or Takyon ROX probe mastermix (Eurogentec UF-RPMT-B0701) and a StepOnePlus Real-Time PCR machine (Applied Biosystems) with StepOne software v. 2.3. Primer sequences, probe sequences and Taqman assays are listed in electronic supplementary material, table S6.

4.12. Collagen antibody ELISA

Tissue culture-treated 96-well plates were coated by incubation with collagen (5 $\mu g\,ml^{-1}$, MD Bioproducts 804001-sol) at 4°C overnight. The plate was washed with PBS containing 0.1% Tween20 (PBS-T), then blocked with 2% BSA in PBS for 1 h. Plates were washed with PBS-T, and then serial dilutions of test plasma samples were added and left at room temperature for 1 h. Plates were washed, incubated with a biotin-conjugated secondary antibody (BD Biosciences, A85-1 (anti-IgG1) or R19–15 (anti-IgG2a)) for 45 min, washed, incubated with streptavidin-HRP (Fisher Scientific 10598893) for 45 min, washed, then incubated with TMB Easy (Fisher Scientific 10499081). Reactions were stopped by the addition of sulphuric acid, and absorbance was read at 405 nm using a GloMax multidetection system (Promega).

4.13. MMP3 ELISA

MMP3 was quantified in serial plasma samples using a Quantikine ELISA kit (Bio Techne MMP300) according to the manufacturer's instructions, with plasma diluted 1 in 25 in calibrant diluent. Plate absorbance was measured on a GloMax multidetection system (Promega).

4.14. Western blotting

FLS were lysed in preheated buffer (2% (w/v) SDS, 10% (v/v) glycerol, 50 mM DTT, 40 mM Tris pH 6.8, 0.001% (w/v) bromophenol blue). Protein samples and standards (Bio-Rad 161–0374) were resolved on TGX stain-free gels (Bio-Rad) run under denaturing conditions, then transferred to nitrocellulose membrane (Sigma-Aldrich GE10600002). Membranes were blocked with 5% (w/v) skimmed milk powder in TBS-T, then incubated overnight with primary antibody (anti-BMAL1, 1/1000, Cell Signaling Technology 14020; anti-β-ACTIN, 1/5000, Sigma-Aldrich A2228). Membranes were washed with TBS-T, incubated with HRP-conjugated secondary antibody, washed and developed using Radiance Plus chemiluminescent substrate (Azure

Biosystems AC2103). Blots were imaged on a ChemiDoc imaging system (Bio-Rad). Uncropped Western blots are shown in electronic supplementary material, figure S6.

4.15. Quantification and statistical analysis

Statistical tests were conducted in GraphPad Prism and are specified in figure legends where appropriate. Throughout, * denotes $p < 0.05$, ** denotes $p < 0.01$, *** denotes $p < 0.001$ and **** denotes $p < 0.0001$.

Ethics. All procedures were approved by the University of Manchester Animal Welfare and Ethical Review Body and carried out according to the Animals (Scientific Procedures) Act 1986 under Home Office project licence numbers P000BBBC3 and PP5819195.

Data accessibility. FLS RNAseq data from this study have been deposited in ArrayExpress with accession code E-MTAB-13317. The scRNAseq data from this study have been deposited with accession code E-MTAB-13320. Published joint RNAseq data used for comparative analysis is available in Gene Expression Omnibus with accession code GSE176095. The analysis code is provided in the electronic supplementary material [78]. Any additional information required to reanalyse the data reported in this paper is available from the corresponding authors upon request.

Declaration of AI use. We have not used AI-assisted technologies in creating this article.

Authors' contributions. P.D.: conceptualization, formal analysis, investigation, methodology, writing—original draft, writing—review and editing; S.H.D.: investigation; D.W.R.: funding acquisition, project administration; D.A.B.: conceptualization, funding acquisition, project administration, supervision, writing—review and editing; J.E.G.: conceptualization, funding acquisition, project administration, supervision, writing—review and editing.

All authors gave final approval for publication and agreed to be held accountable for the work performed therein.

Conflict of interest declaration. We declare we have no competing interests.

Funding. The work was supported by grants from the Medical Research Council (MRC; MR/P023576/1 to D.W.R., D.A.B., J.E.G.; MR/V034049/1 to D.W.R., D.A.B.; MR/W019000/1 to D.W.R.), the Biotechnology and Biological Sciences Research Council (BBSRC; BB/V002651/1 to D.A.B.), Versus Arthritis (22625 to J.E.G.), the Wellcome Trust (107849/Z/15/Z to D.W.R.), the NIHR Oxford Biomedical Research Centre (NIHR203316 to D.W.R.) and a University of Manchester Facilitating Excellence Fund award to P.D.

Acknowledgements. We acknowledge the excellent experimental support of the University of Manchester Core Facilities: Dr Andy Hayes (Genomic Technologies), Dr Leo Zeef and Dr I-Hsuan Lin (Bioinformatics), and Dr Gareth Howell and Mr David Chapman (Flow Cytometry). We also thank and acknowledge the University of Manchester Biological Services Facility staff for animal care, and Dr Edward Hayter for assistance with *in vivo* experiments.

References

1. Aletaha D, Smolen JS. 2018 Diagnosis and management of rheumatoid arthritis: a review. *JAMA* **320**, 1360–1372. (doi:10.1001/jama.2018.13103)
2. Gibbs JE, Ray DW. 2013 The role of the circadian clock in rheumatoid arthritis. *Arthritis Res. Ther.* **15**, 205. (doi:10.1186/ar4146)
3. Hand LE, Dickson SH, Freemont AJ, Ray DW, Gibbs JE. 2019 The circadian regulator Bmal1 in joint mesenchymal cells regulates both joint development and inflammatory arthritis. *Arthritis Res. Ther.* **21**, 5. (doi:10.1186/s13075-018-1770-1)
4. Hand LE, Hopwood TW, Dickson SH, Walker AL, Loudon ASI, Ray DW, Bechtold DA, Gibbs JE. 2016 The circadian clock regulates inflammatory arthritis. *FASEB J.* **30**, 3759–3770. (doi:10.1096/fj.201600353R)
5. Poolman TM *et al*. 2019 Rheumatoid arthritis reprograms circadian output pathways. *Arthritis Res. Ther.* **21**, 47. (doi:10.1186/s13075-019-1825-y)
6. Butler T, Maidstone RJ, Rutter MK, McLaughlin JT, Ray DW, Gibbs JE. 2023 The associations of chronotype and shift work with rheumatoid arthritis. *J. Biol. Rhythms* **38**, 510–518. (doi:10.1177/07487304231179595)
7. Takahashi JS. 2017 Transcriptional architecture of the mammalian circadian clock. *Nat. Rev. Genet.* **18**, 164–179. (doi:10.1038/nrg.2016.150)
8. Patke A, Young MW, Axelrod S. 2020 Molecular mechanisms and physiological importance of circadian rhythms. *Nat. Rev. Mol. Cell Biol.* **21**, 67–84. (doi:10.1038/s41580-019-0179-2)
9. Scheiermann C, Gibbs J, Ince L, Loudon A. 2018 Clocking in to immunity. *Nat. Rev. Immunol.* **18**, 423–437. (doi:10.1038/s41577-018-0008-4)
10. Luross JA, Williams NA. 2001 The genetic and immunopathological processes underlying collagen-induced arthritis. *Immunology* **103**, 407–416. (doi:10.1046/j.1365-2567.2001.01267.x)
11. Downton P *et al*. 2022 Chronic inflammatory arthritis drives systemic changes in circadian energy metabolism. *Proc. Natl Acad. Sci. USA* **119**, e2112781119. (doi:10.1073/pnas.2112781119)
12. Hand LE, Gray KJ, Dickson SH, Simpkins DA, Ray DW, Konkel JE, Hepworth MR, Gibbs JE. 2020 Regulatory T cells confer a circadian signature on inflammatory arthritis. *Nat. Commun.* **11**, 1658. (doi:10.1038/s41467-020-15525-0)
13. Nygaard G, Firestein GS. 2020 Restoring synovial homeostasis in rheumatoid arthritis by targeting fibroblast-like synoviocytes. *Nat. Rev. Rheumatol.* **16**, 316–333. (doi:10.1038/s41584-020-0413-5)
14. Armaka M *et al*. 2022 Single-cell multimodal analysis identifies common regulatory programs in synovial fibroblasts of rheumatoid arthritis patients and modeled TNF-driven arthritis. *Genome Med.* **14**, 78. (doi:10.1186/s13073-022-01081-3)
15. Croft AP *et al*. 2019 Distinct fibroblast subsets drive inflammation and damage in arthritis. *Nature* **570**, 246–251. (doi:10.1038/s41586-019-1263-7)
16. Korsunsky I *et al*. 2022 Cross-tissue, single-cell stromal atlas identifies shared pathological fibroblast phenotypes in four chronic inflammatory diseases. *Med.* **3**, 481–518. (doi:10.1016/j.medj.2022.05.002)
17. Collins FL, Roelofs AJ, Symons RA, Kania K, Campbell E, Collie-Duguid ESR, Riemen AHK, Clark SM, De Bari C. 2023 Taxonomy of fibroblasts and progenitors in the synovial joint at single-cell resolution. *Ann. Rheum. Dis.* **82**, 428–437. (doi:10.1136/ard-2021-221682)
18. Sakurai H, Kohsaka H, Liu MF, Higashiyama H, Hirata Y, Kanno K, Saito I, Miyasaka N. 1995 Nitric oxide production and inducible nitric oxide synthase expression in inflammatory arthritides. *J. Clin. Invest.* **96**, 2357–2363. (doi:10.1172/JCI118292)
19. McInnes IB *et al*. 1996 Production of nitric oxide in the synovial membrane of rheumatoid and osteoarthritis patients. *J. Exp. Med.* **184**, 1519–1524. (doi:10.1084/jem.184.4.1519)

20. Shen P *et al*. 2023 NOS inhibition reverses TLR2-induced chondrocyte dysfunction and attenuates age-related osteoarthritis. *Proc. Natl Acad. Sci. USA* **120**, e2207993120. (doi:10.1073/pnas.2207993120)
21. Yoshihara Y, Nakamura H, Obata K, Yamada H, Hayakawa T, Fujikawa K, Okada Y. 2000 Matrix metalloproteinases and tissue inhibitors of metalloproteinases in synovial fluids from patients with rheumatoid arthritis or osteoarthritis. *Ann. Rheum. Dis*. **59**, 455–461. (doi:10.1136/ard.59.6.455)
22. Perry MG, Kirwan JR, Jessop DS, Hunt LP. 2009 Overnight variations in cortisol, interleukin 6, tumour necrosis factor alpha and other cytokines in people with rheumatoid arthritis. *Ann. Rheum. Dis*. **68**, 63–68. (doi:10.1136/ard.2007.086561)
23. Armaka M, Apostolaki M, Jacques P, Kontoyiannis DL, Elewaut D, Kollias G. 2008 Mesenchymal cell targeting by TNF as a common pathogenic principle in chronic inflammatory joint and intestinal diseases. *J. Exp. Med*. **205**, 331–337. (doi:10.1084/jem.20070906)
24. Kugler M *et al*. 2023 Cytokine-directed cellular cross-talk imprints synovial pathotypes in rheumatoid arthritis. *Ann. Rheum. Dis*. **82**, 1142–1152. (doi:10.1136/ard-2022-223396)
25. Yoshitomi H. 2019 Regulation of immune responses and chronic inflammation by fibroblast-like synoviocytes. *Front. Immunol*. **10**, 1395. (doi:10.3389/fimmu.2019.01395)
26. Mizoguchi F *et al*. 2018 Functionally distinct disease-associated fibroblast subsets in rheumatoid arthritis. *Nat. Commun*. **9**, 789. (doi:10.1038/s41467-018-02892-y)
27. Smith MH *et al*. 2023 Drivers of heterogeneity in synovial fibroblasts in rheumatoid arthritis. *Nat. Immunol*. **24**, 1200–1210. (doi:10.1038/s41590-023-01527-9)
28. Cermakian N, Westfall S, Kiessling S. 2014 Circadian clocks and inflammation: reciprocal regulation and shared mediators. *Arch. Immunol. Ther. Exp.* **62**, 303–318. (doi:10.1007/s00005-014-0286-x)
29. Haspel JA *et al*. 2014 Circadian rhythm reprogramming during lung inflammation. *Nat. Commun*. **5**, 4753. (doi:10.1038/ncomms5753)
30. Cunningham PS, Ahern SA, Smith LC, da Silva Santos CS, Wager TT, Bechtold DA. 2016 Targeting of the circadian clock via CK1delta/epsilon to improve glucose homeostasis in obesity. *Sci. Rep*. **6**, 29983. (doi:10.1038/srep29983)
31. Chen S, Fuller KK, Dunlap JC, Loros JJ. 2020 A pro- and anti-inflammatory axis modulates the macrophage circadian clock. *Front. Immunol.* **11**, 867. (doi:10.3389/fimmu.2020.00867)
32. Kwak Y, Lundkvist GB, Brask J, Davidson A, Menaker M, Kristensson K, Block GD. 2008 Interferon-gamma alters electrical activity and clock gene expression in suprachiasmatic nucleus neurons. *J. Biol. Rhythms* **23**, 150–159. (doi:10.1177/0748730407313355)
33. Grillet B, Pereira RVS, Van Damme J, Abu El-Asrar A, Proost P, Opdenakker G. 2023 Matrix metalloproteinases in arthritis: towards precision medicine. *Nat. Rev. Rheumatol*. **19**, 363–377. (doi:10.1038/s41584-023-00966-w)
34. Fingleton B. 2017 Matrix metalloproteinases as regulators of inflammatory processes. *Biochim. Biophys. Acta Mol. Cell Res*. **1864**, 2036–2042. (doi:10.1016/j.bbamcr.2017.05.010)
35. Tolboom TCA, Pieterman E, van der Laan WH, Toes REM, Huidekoper AL, Nelissen RGHH, Breedveld FC, Huizinga TWJ. 2002 Invasive properties of fibroblast-like synoviocytes: correlation with growth characteristics and expression of MMP-1, MMP-3, and MMP-10. *Ann. Rheum. Dis*. **61**, 975–980. (doi:10.1136/ard.61.11.975)
36. Ogata Y, Enghild JJ, Nagase H. 1992 Matrix metalloproteinase 3 (stromelysin) activates the precursor for the human matrix metalloproteinase 9. *J. Biol. Chem*. **267**, 3581–3584.
37. Wan J, Zhang G, Li X, Qiu X, Ouyang J, Dai J, Min S. 2021 Matrix metalloproteinase 3: a promoting and destabilizing factor in the pathogenesis of disease and cell differentiation. *Front. Physiol*. **12**, 663978. (doi:10.3389/fphys.2021.663978)
38. Bove PF, Wesley UV, Greul AK, Hristova M, Dostmann WR, van der Vliet A. 2007 Nitric oxide promotes airway epithelial wound repair through enhanced activation of MMP-9. *Am. J. Respir. Cell Mol. Biol*. **36**, 138–146. (doi:10.1165/rcmb.2006-0253SM)
39. Cunningham PS *et al*. 2023 ClinCirc identifies alterations of the circadian peripheral oscillator in critical care patients. *J. Clin. Invest*. **133**, e162775. (doi:10.1172/JCI162775)
40. Zhao J *et al*. 2018 BMAL1 deficiency contributes to mandibular dysplasia by upregulating MMP3. *Stem Cell Rep.* **10**, 180–195. (doi:10.1016/j.stemcr.2017.11.017)
41. Yang W *et al*. 2016 Clock gene Bmal1 modulates human cartilage gene expression by crosstalk with Sirt1. *Endocrinology* **157**, 3096–3107. (doi:10.1210/en.2015-2042)
42. Liu H *et al*. 2020 NR1D1 modulates synovial inflammation and bone destruction in rheumatoid arthritis. *Cell Death Dis*. **11**, 129. (doi:10.1038/s41419-020-2314-6)
43. Lam MTY *et al*. 2013 Rev-Erbs repress macrophage gene expression by inhibiting enhancer-directed transcription. *Nature* **498**, 511–515. (doi:10.1038/nature12209)
44. Zheng R *et al*. 2019 Cistrome data browser: expanded datasets and new tools for gene regulatory analysis. *Nucleic Acids Res*. **47**, D729–D735. (doi:10.1093/nar/gky1094)
45. Sasaki S, Iwata H, Ishiguro N, Obata K, Miura T. 1994 Detection of stromelysin in synovial fluid and serum from patients with rheumatoid arthritis and osteoarthritis. *Clin. Rheumatol*. **13**, 228–233. (doi:10.1007/BF02249017)
46. Sun S, Bay-Jensen AC, Karsdal MA, Siebuhr AS, Zheng Q, Maksymowych WP, Christiansen TG, Henriksen K. 2014 The active form of MMP-3 is a marker of synovial inflammation and cartilage turnover in inflammatory joint diseases. *BMC Musculoskelet. Disord*. **15**, 93. (doi:10.1186/1471-2474-15-93)
47. Houseman M, Potter C, Marshall N, Lakey R, Cawston T, Griffiths I, Young-Min S, Isaacs JD. 2012 Baseline serum MMP-3 levels in patients with rheumatoid arthritis are still independently predictive of radiographic progression in a longitudinal observational cohort at 8 years follow up. *Arthritis Res. Ther*. **14**, R30. (doi:10.1186/ar3734)
48. Lerner A, Neidhöfer S, Reuter S, Matthias T. 2018 MMP3 is a reliable marker for disease activity, radiological monitoring, disease outcome predictability, and therapeutic response in rheumatoid arthritis. *Best Pract. Res. Clin. Rheumatol*. **32**, 550–562. (doi:10.1016/j.berh.2019.01.006)
49. Humby F *et al*. 2019 Synovial cellular and molecular signatures stratify clinical response to csDMARD therapy and predict radiographic progression in early rheumatoid arthritis patients. *Ann. Rheum. Dis*. **78**, 761–772. (doi:10.1136/annrheumdis-2018-214539)
50. Park JK *et al*. 2020 Therapeutic potential of CKD-506, a novel selective histone deacetylase 6 inhibitor, in a murine model of rheumatoid arthritis. *Arthritis Res. Ther*. **22**, 176. (doi:10.1186/s13075-020-02258-0)
51. Svensson MND *et al*. 2020 Synoviocyte-targeted therapy synergizes with TNF inhibition in arthritis reversal. *Sci. Adv*. **6**, eaba4353. (doi:10.1126/sciadv.aba4353)
52. Kaneko K, Williams RO, Dransfield DT, Nixon AE, Sandison A, Itoh Y. 2016 Selective inhibition of membrane type 1 matrix metalloproteinase abrogates progression of experimental inflammatory arthritis: synergy with tumor necrosis factor blockade. *Arthritis Rheumatol*. **68**, 521–531. (doi:10.1002/art.39414)
53. Ding Q *et al*. 2023 Signaling pathways in rheumatoid arthritis: implications for targeted therapy. *Signal Transduct. Target. Ther*. **8**, 68. (doi:10.1038/s41392-023-01331-9)
54. Hergenhan S, Holtkamp S, Scheiermann C. 2020 Molecular interactions between components of the circadian clock and the immune system. *J. Mol. Biol*. **432**, 3700–3713. (doi:10.1016/j.jmb.2019.12.044)
55. Gibbs J *et al*. 2014 An epithelial circadian clock controls pulmonary inflammation and glucocorticoid action. *Nat. Med*. **20**, 919–926. (doi:10.1038/nm.3599)
56. Pariollaud M *et al*. 2018 Circadian clock component REV-ERBalpha controls homeostatic regulation of pulmonary inflammation. *J. Clin. Invest*. **128**, 2281–2296. (doi:10.1172/JCI93910)
57. Sutton CE, Finlay CM, Raverdeau M, Early JO, DeCourcey J, Zaslona Z, O'Neill LAJ, Mills KHG, Curtis AM. 2017 Loss of the molecular clock in myeloid cells exacerbates T cell-mediated CNS autoimmune disease. *Nat. Commun*. **8**, 1923. (doi:10.1038/s41467-017-02111-0)
58. Schlenner S *et al*. 2019 NFIL3 mutations alter immune homeostasis and sensitise for arthritis pathology. *Ann. Rheum. Dis*. **78**, 342–349. (doi:10.1136/annrheumdis-2018-213764)
59. Bekki H, Duffy T, Okubo N, Olmer M, Alvarez-Garcia O, Lamia K, Kay S, Lotz M. 2020 Suppression of circadian clock protein cryptochrome 2 promotes osteoarthritis. *Osteoarthr. Cartil*. **28**, 966–976. (doi:10.1016/j.joca.2020.04.004)

60. Hashiramoto A *et al*. 2010 Mammalian clock gene cryptochrome regulates arthritis via proinflammatory cytokine TNF-alpha. *J. Immunol*. **184**, 1560–1565. (doi:10.4049/jimmunol.0903284)
61. Damerau A, Gaber T. 2020 Modeling rheumatoid arthritis in vitro: from experimental feasibility to physiological proximity. *Int. J. Mol. Sci*. **21**, 7916. (doi:10.3390/ijms21217916)
62. Chang J *et al*. 2020 Circadian control of the secretory pathway maintains collagen homeostasis. *Nat. Cell Biol*. **22**, 74–86. (doi:10.1038/s41556-019-0441-z)
63. Dudek M, Morris H, Rogers N, Pathiranage DR, Raj SS, Chan D, Kadler KE, Hoyland J, Meng QJ. 2023 The clock transcription factor BMAL1 is a key regulator of extracellular matrix homeostasis and cell fate in the intervertebral disc. *Matrix Biol*. **122**, 1–9. (doi:10.1016/j.matbio.2023.07.002)
64. Nagler-Anderson C, Bober LA, Robinson ME, Siskind GW, Thorbecke GJ. 1986 Suppression of type II collagen-induced arthritis by intragastric administration of soluble type II collagen. *Proc. Natl Acad. Sci. USA* **83**, 7443–7446. (doi:10.1073/pnas.83.19.7443)
65. Yoshinari O, Shiojima Y, Moriyama H, Shinozaki J, Nakane T, Masuda K, Bagchi M. 2013 Water-soluble undenatured type II collagen ameliorates collagen-induced arthritis in mice. *J. Med. Food* **16**, 1039–1045. (doi:10.1089/jmf.2013.2911)
66. Sun G, Hou Y, Gong W, Liu S, Li J, Yuan Y, Zhang D, Chen Q, Yan X. 2018 Adoptive induced antigen-specific treg cells reverse inflammation in collagen-induced arthritis mouse model. *Inflammation* **41**, 485–495. (doi:10.1007/s10753-017-0704-4)
67. Madisen L *et al*. 2012 A toolbox of Cre-dependent optogenetic transgenic mice for light-induced activation and silencing. *Nat. Neurosci*. **15**, 793–802. (doi:10.1038/nn.3078)
68. Bolger AM, Lohse M, Usadel B. 2014 Trimmomatic: a flexible trimmer for Illumina sequence data. *Bioinformatics* **30**, 2114–2120. (doi:10.1093/bioinformatics/btu170)
69. Dobin A, Davis CA, Schlesinger F, Drenkow J, Zaleski C, Jha S, Batut P, Chaisson M, Gingeras TR. 2013 STAR: ultrafast universal RNA-seq aligner. *Bioinformatics* **29**, 15–21. (doi:10.1093/bioinformatics/bts635)
70. Love MI, Huber W, Anders S. 2014 Moderated estimation of fold change and dispersion for RNA-seq data with DESeq2. *Genome Biol*. **15**, 550. (doi:10.1186/s13059-014-0550-8)
71. Xie Z *et al*. 2021 Gene set knowledge discovery with enrichr. *Curr. Protoc*. **1**, e90. (doi:10.1002/cpz1.90)
72. Amezquita RA *et al*. 2020 Orchestrating single-cell analysis with bioconductor. *Nat. Methods* **17**, 137–145. (doi:10.1038/s41592-019-0654-x)
73. McCarthy DJ, Campbell KR, Lun ATL, Wills QF. 2017 Scater: pre-processing, quality control, normalization and visualization of single-cell RNA-seq data in R. *Bioinformatics* **33**, 1179–1186. (doi:10.1093/bioinformatics/btw777)
74. Lun ATL, McCarthy DJ, Marioni JC. 2016 A step-by-step workflow for low-level analysis of single-cell RNA-seq data with Bioconductor. *F1000Res*. **5**, 2122. (doi:10.12688/f1000research.9501.2)
75. Haghverdi L, Lun ATL, Morgan MD, Marioni JC. 2018 Batch effects in single-cell RNA-sequencing data are corrected by matching mutual nearest neighbors. *Nat. Biotechnol*. **36**, 421–427. (doi:10.1038/nbt.4091)
76. Robinson MD, McCarthy DJ, Smyth GK. 2010 edgeR: a Bioconductor package for differential expression analysis of digital gene expression data. *Bioinformatics* **26**, 139–140. (doi:10.1093/bioinformatics/btp616)
77. Chen Y, Lun ATL, Smyth GK. 2016 From reads to genes to pathways: differential expression analysis of RNA-Seq experiments using Rsubread and the edgeR quasi-likelihood pipeline. *F1000Res*. **5**, 1438. (doi:10.12688/f1000research.8987.2)
78. Downton P, Dickson SH, Ray DW, Bechtold DA, Gibbs JE. 2024 Supplementary material from: Fibroblast-like synoviocytes orchestrate daily rhythmic inflammation in arthritis. Figshare. (doi:10.6084/m9.figshare.c.7303177)